

Numerical analysis of microwave heating cavity

Combining electromagnetic energy, heat transfer and fluid dynamics for a NaY zeolite fixed-bed

Nigar, H.; Sturm, G. S.J.; Garcia-Baños, B.; Peñaranda-Foix, F. L.; Catalá-Civera, J. M.; Mallada, R.; Stankiewicz, A.; Santamaría, J.

DOI

[10.1016/j.applthermaleng.2019.03.117](https://doi.org/10.1016/j.applthermaleng.2019.03.117)

Publication date

2019

Document Version

Final published version

Published in

Applied Thermal Engineering

Citation (APA)

Nigar, H., Sturm, G. S. J., Garcia-Baños, B., Peñaranda-Foix, F. L., Catalá-Civera, J. M., Mallada, R., Stankiewicz, A., & Santamaría, J. (2019). Numerical analysis of microwave heating cavity: Combining electromagnetic energy, heat transfer and fluid dynamics for a NaY zeolite fixed-bed. *Applied Thermal Engineering*, 155, 226-238. <https://doi.org/10.1016/j.applthermaleng.2019.03.117>

Important note

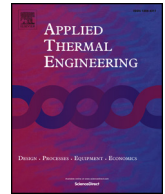
To cite this publication, please use the final published version (if applicable).
Please check the document version above.

Copyright

Other than for strictly personal use, it is not permitted to download, forward or distribute the text or part of it, without the consent of the author(s) and/or copyright holder(s), unless the work is under an open content license such as Creative Commons.

Takedown policy

Please contact us and provide details if you believe this document breaches copyrights.
We will remove access to the work immediately and investigate your claim.



Research Paper

Numerical analysis of microwave heating cavity: Combining electromagnetic energy, heat transfer and fluid dynamics for a NaY zeolite fixed-bed

H. Nigar^a, G.S.J. Sturm^b, B. Garcia-Baños^c, F.L. Peñaranda-Foix^c, J.M. Catalá-Civera^c, R. Mallada^{a,d,e,*}, A. Stankiewicz^b, J. Santamaría^{a,d,e,*}

^a Nanoscience Institute of Aragon and Chemical and Environmental Engineering Department, University of Zaragoza, 50018 Zaragoza, Spain

^b Process & Energy Department, Delft University of Technology, Leegwaterstraat 39, 2628 CB Delft, the Netherlands

^c Instituto ITACA, Universitat Politècnica de València, Camino de Vera, 46022 Valencia, Spain

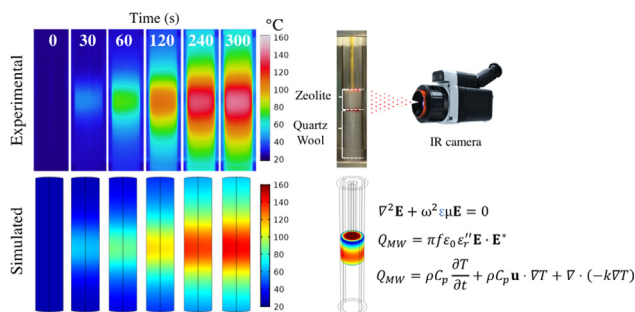
^d Networking Research Centre CIBER-BBN, 28029 Madrid, Spain

^e Instituto de Ciencia de Materiales de Aragón, CSIC-Universidad de Zaragoza, C/ Pedro Cerbuna 12, E-50.009 Zaragoza, Spain

HIGHLIGHTS

- Electromagnetic, heat transfer and fluid dynamics coupled for MW heating simulation.
- Dielectric properties of NaY zeolite measured as a function of temperature 298–623 K.
- Temperature evolution and distribution results validated with experimental data.
- Model predicts thermal runaway of zeolite under MW heating.

GRAPHICAL ABSTRACT



ARTICLE INFO

Keywords:

Modelling and numerical simulation
Dielectric properties
Microwave heating
Power dissipation
Transient temperature profiles

ABSTRACT

Three-dimensional mathematical model was developed for a rectangular TE_{10n} microwave heating cavity system, working at 2.45 GHz. Energy/heat, momentum equations were solved together with Maxwell's electromagnetic field equations using COMSOL MULTIPHYSICS® simulation environment. The dielectric properties, ϵ' and ϵ'' , of NaY zeolite (Si/Al = 2.5) were evaluated as a function of temperature. Considering these values, the microwave heating of a porous fixed-bed made of dry NaY zeolite was simulated. Electric field distribution, axial and radial temperature profiles and temperature evolution with time were obtained. The zeolite fixed bed was heated up to 180 °C in 5 min, with 30 W power. The fixed-bed temperature evolution under non-steady state conditions showed the same trend as the one observed experimentally with only an average deviation of 10.3%. The model was used to predict microwave heating of other materials improving energy efficiency of the microwave cavity. Furthermore, the developed model was able to predict thermal runaway for zeolites.

* Corresponding authors at: Institute of Nanoscience of Aragon, Universidad de Zaragoza, C/Mariano Esquillor s/n, 50018 Zaragoza, Spain.

E-mail addresses: rmallada@unizar.es (R. Mallada), jesus.santamaria@unizar.es (J. Santamaría).

Nomenclature			
C_p	heat capacity (J/kg K)	ϵ_0	permittivity of free space (F/m)
D	diameter (m)	ϵ_r	relative permittivity (–)
\mathbf{E}	electric field vector (V/m)	ϵ_r''	relative dielectric constant (–)
f	Frequency (Hz)	ϵ_r'''	relative dielectric loss factor (–)
\mathbf{g}	Gravitational acceleration (m/s ²)	ϵ	bed porosity (–)
Gr	Grashof number	η	viscosity (Pa s)
k	thermal conductivity (W/m K)	κ	bed permeability (m ²)
H	height (m)	μ	permeability (H/m)
p	pressure (Pa)	μ_r	relative permeability (–)
Pr	Prandtl number	η	viscosity (Pa s)
Ra	Rayleigh Number	ρ	density (kg/m ³)
T	temperature (°C)	ω	angular frequency (rad/s)
t	time (s)		
TE	transverse electric mode	<i>Subscripts</i>	
TM	transverse magnetic mode	bed	NaY zeolite load
\mathbf{u}	flow velocity vector field for the x, y, z directions	eff	effective
Q_{MW}	volumetric microwave power dissipation (W/m ³)	i	inner
		o	outer
		ref	reference
		w	Quartz wall
<i>Greek Symbols</i>			
ϵ	permittivity (F/m)		

1. Introduction

Microwave heating, MWH, directly converts the microwave energy into heat in contrast to conventional heating. CH, transfer mechanisms that occur through a surface. The electromagnetic waves directly interact with the charges in the molecules and solids (i.e., dipoles, ions or delocalized electrons) which result in a volumetric heating of the material. MWH is characterized by a non-contact, rapid and selective heating that leads to shorter processing times. MWH is considered as an energy efficient process; although there is still some controversy on this aspect [1,2]. Nevertheless the importance and efficiency of MWH technology is endorsed by many different processing industries, starting from food technology, material processing and sintering, coal and mining that routinely heat by microwaves as a well-established technology [3,4]. In the last fifteen years the advances in microwave assisted synthesis/chemistry including organic synthesis and heterogeneous catalysis are becoming more important and microwave energy is presented as a tool for green chemistry [2] and process intensification [5].

Microwave driven chemical reactors often report better performance compared to its counterparts heated by conventional methods, but most of the times the differences are related with the so-called “thermal effects”, and several studies point out the non-uniform heat generation with microwave irradiation due to the spatial variations of the electromagnetic field within the sample [6–8] or non-homogeneous distribution of the material [9]. The non-uniform heating and temperature distribution can be overcome in the case of liquids basically by stirring; however, the problem still remains in the case of continuous flow reactors, and heterogeneous solid-gas phase catalytic systems. Especially, the temperature distribution within the fixed/packed-bed configuration is important for the conversion of the reactants of interest. Durka et al. [6] reported significant two-dimensional temperature gradients in a fixed-bed of CuZnO/Al₂O₃ catalysts both in axial and radial directions. They observed 60 °C difference from bottom to top in 12 mm length, and 25–45 °C from center to the wall in 24 mm of diameter. A recent work of Horikoshi et al. [10] focused on the selective heating of Pd/Activated Carbon catalyst in heterogeneous systems via microwave heating for continuous evolution of hydrogen from organic hydrides. They observed a large temperature distribution along the 50 mm length of the catalytic bed. Almost a 50% drop in temperature

below the 15 mm of the catalytic bed, where the dehydrogenation reaction could not take place due to the lower temperature. They claim that a more uniform distribution of electromagnetic field should lead to more uniform temperature within the catalyst bed and could result in significant improvement in process efficiency while giving a high conversion yields and considerable energy saving compared to the conventional heating.

The spatial electric and magnetic field distribution inside a microwave cavity, as well as in the material processed, are the major factors for materials processing to obtain the temperature profiles of the heated sample. The study of temperature distribution in microwave heated solids has been addressed by several authors, focused on the non-uniform temperature distribution, hot and/or cold spots inside the heated material by microwave [11–18]. The numerical models include the simultaneous solution of differential equations for the electromagnetic field distribution, heat transfer and fluid dynamics with a finite element analysis. To perform the simulation, the exact geometry of the cavity and material together with its three-dimensional position within the cavity are essential. The temperature gradients simulated in the case of heating pinewood, carbon, Pyrex and combinations of thereof could be as high as 800 K in the case of carbon cylinders inside a wood cube of 86 mm side, from the outer side to the inner part [14]. Unfortunately, none of the works were able to validate the simulated temperature profiles with experimental temperature distribution in a 2D map. Furthermore, in all the cases constant values for the dielectric properties with temperature have been considered, but this could be of special relevance in the case of important changes on these properties that could lead to a runaway.

Zeolites are hydrated aluminosilicates with a three-dimensional pore structure containing cations in exchange positions. The number of these cations in zeolites depends on the Si/Al ratio of the zeolite. As soon as the tetrahedrally coordinated Si is replaced by Al, a charged defect is created that is compensated by an extra-framework cation. NaY zeolite belongs to the Faujasite (FAU) type possess a spherical supercage which is assembled by sodalite cages, developing a maximum diameter of 1.12 nm with an aperture of 0.71–0.73 nm. Extra-framework cations, Na⁺, are located within the cages to keep the overall framework neutral. These microporous materials have a high porosity and elevated surface area and are very well known as catalysts, catalytic supports, adsorbents and ion-exchangers [19,20]. During the

regeneration of sorbents or in the catalytic processes it is necessary to supply heat to these materials, and the use of microwaves as alternative way of heating it is presented as an opportunity. As an example, in our previous works, we studied microwave heated fixed beds of FAU zeolite in adsorption [21], and in catalysis [22] for the removal of volatile organic compounds, VOCs.

In the present work, microwave heating of a dry porous zeolite fixed-bed in a quartz tube was studied both experimentally and

numerically in a mono-mode rectangular resonant cavity. The focus was on the study of the electric field distribution, heat generation, heat transfer, and temperature distribution. The COMSOL Multiphysics® (version 5.2.) simulation environment was used to perform the three-dimensional modelling of a mono-mode (TE₁₀) rectangular waveguide microwave heating cavity. The temperature distribution in time and space within the sample in a fixed-bed configuration was simulated in the basis of experimentally measured dielectric properties (ϵ' and ϵ'') of

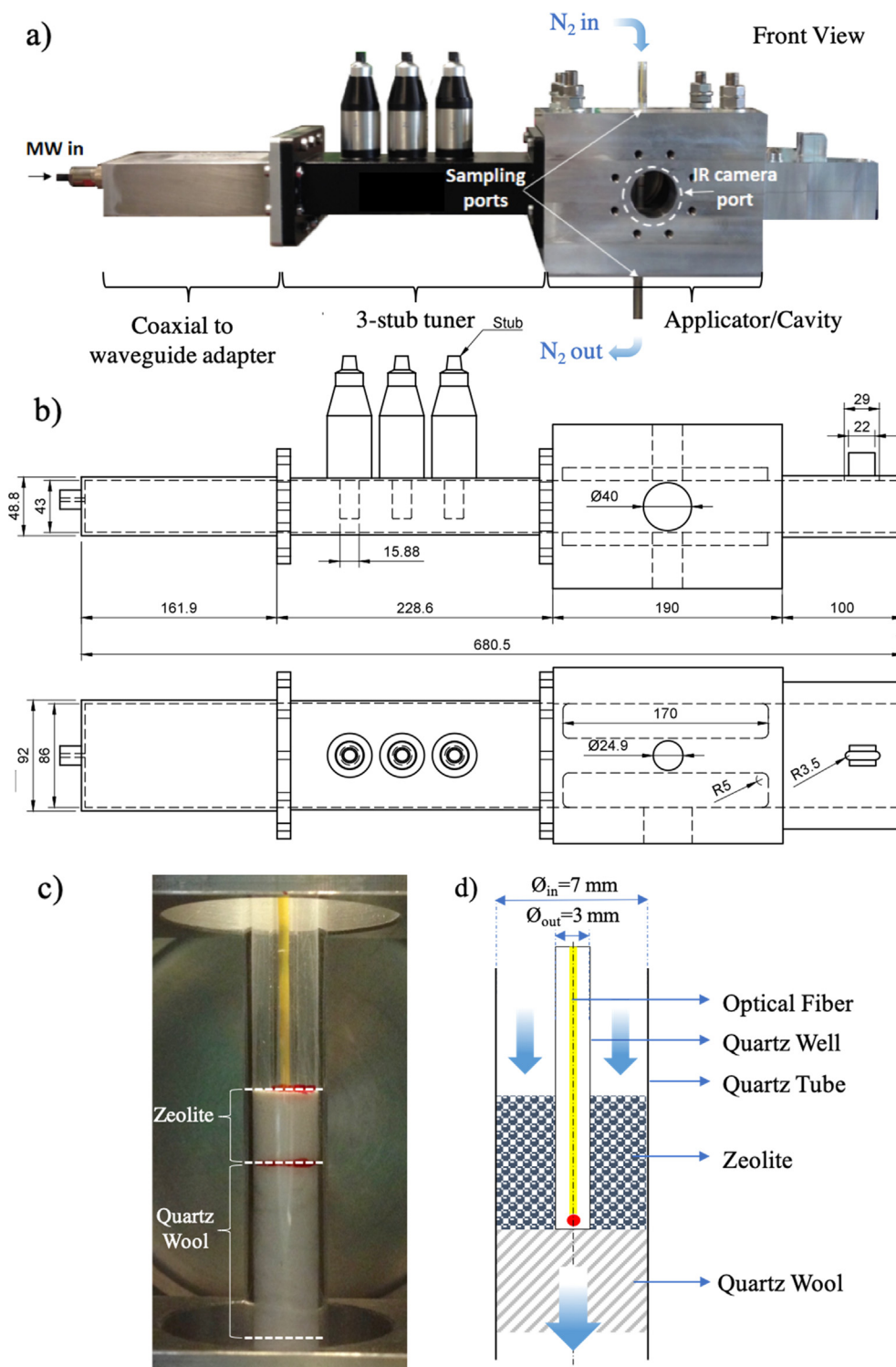


Fig. 1. Experimental setup, (a) Microwave heating cavity (b) The first-angle projection of 3D modelled empty Microwave Heating Cavity, the dashed lines indicate hidden edges and corners, measurement in mm (c) Fixed-bed quartz tube and its corresponding (d) schematic view.

the NaY zeolite as a function of temperature. The simulated temperature profiles were then validated with experimental data obtained with a fiber optic sensor and thermographic camera and the model was used to predict possible runaway during microwave heating of zeolites as well as the heating behavior of other materials inside the cavity.

2. Experimental system

The microwave heating cavity, see Fig. 1a, was supplied by Sairem Iberica and consist of a solid-state microwave generator functioning at the range of 2.43–2.47 GHz with a 0.1 MHz step and a maximum power of 150 W, and a TE₁₀ mode microwave cavity with a WR340

waveguide. The cavity was further modified with a precision 3-Stub Tuner (GA1002 model, Gerling Applied Engineering, Inc., USA) to reduce the reflected power below than 10% of the forward power. Before starting the experiments, the cavity was tuned and the mismatch was analyzed by the evaluation of S-parameters, S₁₁, which are obtained by a Network Analyzer (Agilent E5061B 5 Hz–3 GHz) within the frequency range of 2.43–2.47 GHz with 0.1 MHz steps.

A fixed-bed quartz tube ($\varnothing_{in-out} = 7-9$ mm) was located inside the cavity through two circular sampling ports (top and bottom). The temperature in the fixed-bed was measured with a fiber optic sensor (range: -80 to 250 °C, $\varnothing:1$ mm, Neoptix T1 Probe) inside a capillary quartz well, see Fig. 1c. The temperatures reported in this work for the

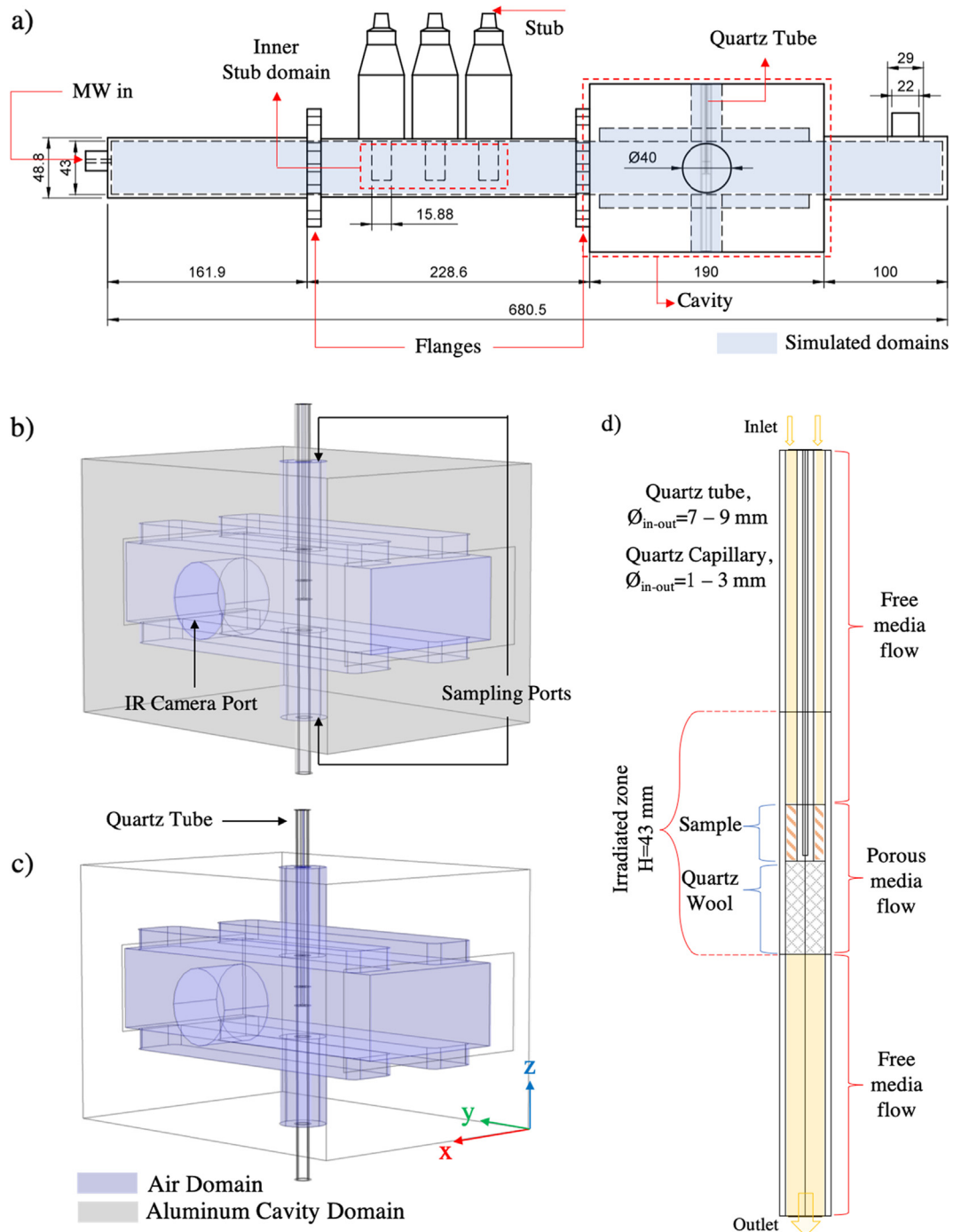


Fig. 2. Cross-sectional and perspective views of (a) simulated domains (b) aluminum cavity domain (c) air domain and (d) quartz tube and applied flow models, i.e., laminar, free and porous media flows.

Table 1
Characteristics of the simulated system.

Fixed-Bed	Value	Refs.
Height, H (m)	0.010	–
Inner diameter, D _i (m)	0.007	–
Outer diameter, D _o (m)	0.009	–
Bed density, ρ_{bed} (kg m ⁻³)	672	–
Bed porosity, ϵ_{bed} (–)	0.375 ^a	[33]
Bed permeability, κ_{bed} (m ²)	1.15×10^{-11b}	[34]
<i>NaY Zeolite (Si/Al = 2.5)</i>		
Average diameter, d_{NaY} (m)	1.15×10^{-4}	–
Dielectric constant, ϵ'_{NaY} (–)	f(T) ^c	–
Loss factor ϵ''_{NaY} (–)		
Heat capacity, $C_{p,NaY}$ (J kg ⁻¹ K ⁻¹)	836	[35]
Thermal conductivity, k_{NaY} (W m ⁻¹ K ⁻¹)	0.15	[30]
<i>Quartz Tube and Quartz Wool</i>		
Quartz density, ρ_w (kg m ⁻³)	2200	[36]
Dielectric constant, ϵ'_r (–)	3.78	[36]
Heat capacity, $C_{p,w}$ (J kg ⁻¹ K ⁻¹)	712	[36]
Thermal conductivity, k_w (W m ⁻¹ K ⁻¹)	1.96	[37]
<i>Air and Nitrogen</i>		
Dielectric constant, ϵ'_r (–)	1	–
Loss factor ϵ''_r (–)	0	–
Density, Heat capacity and Thermal conductivity	See supporting Information	

^a Calculated using empirical expression of Pushnov for sphere grains.

^b Calculated using empirical expression of Rumpf and Gupte for sphere packings.

^c Experimentally measured at 2.45 GHz as a function of temperature, cooling cycle data were used.

fixed bed experiments correspond to the fiber optic sensor readings at the bottom of the fixed-bed. The surface temperature of the quartz tube was also measured by an infrared thermographic camera, (range: 0–500 °C, InfraTec, GmbH, quartz emissivity: 0.9 according to camera manual) located in front of the side window of the cavity. The Infrared camera captures the infrared images every 3 s. The images are further processed with an algorithm that has been developed with the Image Processing Toolbox[®] of MATLAB to extract the quartz tube surface temperature, e.g., transient average, maximum or both. Fig. 1 shows in detail the experimental setup of the microwave heating cavity with the dimensions and the fixed-bed configuration.

The heated solid was a commercial zeolite Y powder, CBV100, (Si/Al = 2.5) supplied by Zeolyst, containing 13.0 wt% of Na⁺ as an extra-framework cation. The fine powder, without any post-treatment, was first pelletized with a laboratory press using a stainless-steel mold (13 mm in diameter). Then the pellets were crushed and ground to 80–150 μm in order to prevent compaction of the fixed bed (200 mg, 80–150 μm, L = 10 mm, ϕ_{in} = 7 mm). Before the heating experiments, the fixed-bed was regenerated by microwave heating while passing N₂ (100 mL/min, 99.9999% pure, Praxair), meanwhile, the water concentration was registered by an on-line quadrupole mass spectrometer (OmniStar, GSD 320, Pfeiffer Vacuum) to ensure that total dehydration of the sample was reached for a given set of conditions.

2.1. Dynamic measurement of dielectric properties

The ability of a material to absorb microwave energy and transfer it into heat is governed by its dielectric properties [23]. The complex relative permittivity is defined as:

$$\epsilon_r = (\epsilon'_r - j\epsilon''_r) \quad (1)$$

where ϵ'_r is the real part of the complex relative permittivity is known as dielectric constant, which characterizes the electrical polarization of a material in response to an applied external electric field and it is also a measure of dielectric materials to ability to store electrical energy

[24–26], whereas the imaginary part, ϵ''_r , is the dielectric loss factor also known as dissipation factor, which reflects the electromagnetic dissipation in the medium due to damping of the vibrating dipole moments, which generates heat [26,27]. These properties are crucial for the prediction of the spatial distribution and dissipation of electromagnetic wave fields. It is a challenging task to obtain sufficiently accurate values since they are highly dependent on temperature, moisture, frequency, the physical state either solid or liquid and composition [3,25].

Dielectric properties (ϵ'_r and ϵ''_r) of zeolites were measured with a dual-mode microwave system recently developed by Catala-Givera et al. [23]. The equipment allows dielectric measurements of materials during microwave heating in real time. Two separate microwave sources are used for simultaneously heating and measuring, and a cross-coupling filter is used to isolate the two modes (TE₁₁₁ and TM₀₁₀) from each other.

As the dielectric properties of the samples depend on temperature, the resonant frequency and quality factor of the cavity varies with temperature. From these two values, the dielectric properties of the sample are computed with an enhanced Cavity Perturbation Method [23]. To ensure an efficient power delivery and to maintain the desired heating rate a control loop ensures that, the sweep frequency bandwidth of the heating source is adjusted continuously to track the resonant peak of the cavity during the heating cycle.

The sample is inserted into the cavity through a cut-off hole at the central plane of the top wall. The test sample is placed in a quartz vial with inner diameter 10 mm and external diameter 12 mm, which can handle temperatures of up to 1300 °C. The zeolite sample has a bed size of 10 mm diameter and 15 mm height to ensure a uniform electric field distribution in the whole sample volume and thus uniform processing. The temperature of the sample under test is measured by an infrared radiation (IR) thermometer with 0.1 °C accuracy, positioned outside of the cavity and connected to it via a window in the sidewall. Since the IR thermometer measures the holder surface temperature, a calibration process was applied to find the relationship with the bulk temperature of the sample [23]. Before any measurement, the zeolite was dried overnight in an oven at 250 °C; then the measurements were done with a cycle of heating and cooling of the sample under nitrogen flow to minimize the effect of adsorbed ambient moisture. Additionally, a cycle of heating and cooling was performed to ensure complete drying.

3. Mathematical model

The three-dimensional finite element model couples together electromagnetic waves, heat transfer and fluid dynamics. Fig. 2 shows the perspective and cross-sectional views of the model, implemented flow models, and dimensions of the quartz tube and Table 1 represents the characteristics of the simulated system. The flanges and the outer parts of the stub tuner were not included into the model, see Fig. 2a.

The following governing equations were used for each physics module:

3.1. Electromagnetic waves

Maxwell's electromagnetic field distribution and the general volumetric power dissipation are calculated by solving the following equations [26–28]:

$$\nabla^2 \mathbf{E} + \omega^2 \epsilon \mu \mathbf{E} = 0 \quad (2)$$

$$Q_{MW} = \pi f \epsilon_0 \epsilon''_r \mathbf{E} \cdot \mathbf{E}^* \quad (3)$$

where \mathbf{E} (V/m) is the electric field vector, \mathbf{E}^* is the complex conjugate of \mathbf{E} , $\omega = 2\pi f$ (rad/s) is the angular frequency, and ϵ , μ stands for the permittivity and permeability of the media.

The wave equation, Eq. (2), is solved inside the microwave heating cavity (air domain), zeolite fixed-bed and quartz tube, in this physics

interface some assumptions have been made:

- i. Since there is no magnetic material, the magnetic permeability of all the materials is assigned as free-space, $\mu_r = 1$, which gives no magnetic field contribution for the volumetric power dissipation.
- ii. Since the electromagnetic field penetrates a negligible distance into the metallic walls, the three-dimensional wave equation is only applied in the air domain, inside of the waveguide, and inside the fixed-bed and quartz tube, see Fig. 2a. It was found by preliminary modeling that the energy balance was not correctly represented if a perfect electrical conductor (PEC) boundary condition was employed due to the relatively low electromagnetic dissipation inside the fixed-bed. Thus, an impedance boundary condition (IBC) was assigned to the metal walls of the microwave heating cavity to account for the electric surface current present in them.
- iii. Experimentally measured dielectric properties, ϵ' and ϵ'' , of the sample are introduced as a function of temperature.

3.2. Heat transfer

This module is applied inside the microwave heating cavity (air domain), as well as the fixed-bed and the quartz tube walls. Heat transport equation incorporates the conversion of microwave energy to thermal energy, as well as the thermal losses to the environment through the quartz tube walls. In this physic interface, the following transient equation is solved for the porous fixed-bed (solid–fluid system), quartz tube walls and surrounding air [29] simultaneously:

$$\rho C_p \frac{\partial T}{\partial t} + \rho C_p \mathbf{u} \cdot \nabla T + \nabla \cdot (-k \nabla T) = Q_{MW} \quad (4)$$

where ρ, C_p, k are the density, heat capacity and thermal conductivity of the fluid/solid, respectively. The symbol $\mathbf{u} = (u, v, w)$ stands for the flow velocity vector field for the x, y, z directions. First term on the left side is the rate of heat accumulation, and the second and third terms are convective and conductive contributions to heat transfer. On the right-hand side is the volumetric power dissipation, which was calculated with the *Electromagnetic Waves* module. The following assumptions in this module have been made:

- i. The Eq. (4) was modified for the heat transfer in a porous matrix filled with a fluid, introducing an effective volumetric heat capacity, $(\rho C_p)_{eff}$, at constant pressure and effective thermal conductivity, k_{eff} . Both $(\rho C_p)_{eff}$ and k_{eff} were defined by an averaging model, with the following equations, to account for both solid matrix (i.e., NaY) and

fluid (i.e., N_2).

$$(\rho C_p)_{eff} = \theta_p \rho_{NaY} C_{p,NaY} + (1 - \theta_p) \rho_{N_2} C_{p,N_2} \quad (4.1)$$

$$k_{eff} = \theta_p k_{NaY} + (1 - \theta_p) k_{N_2} \quad (4.2)$$

- ii. In the quartz tube walls, only conduction phenomenon was considered.
- iii. Material properties such as thermal conductivity and the heat capacity of the zeolite are considered temperature independent.
- iv. The sampling and IR camera ports, see Figs. 1a and 2a, were assigned as open boundaries to limit a modeling domain that extends in an open fashion. With this condition the heat can flow out of the domain or into the domain with a specified exterior temperature.
- v. A continuity condition was applied to the interface between two different domains 1 and 2: $-n \cdot (-k_1 \nabla T_1) - n \cdot (-k_2 \nabla T_2) = 0$ [30].
- vi. The convective velocity field around the fixed-bed quartz tube can be simulated with fluid dynamics to account for natural convection, see Fig. 2b.
- vii. Fixed temperature, i.e., 20 °C, can be assigned for the metallic walls of the cavity.

3.3. Fluid dynamics

Two physics interfaces were used in this module; *Free and Porous Media Flow* was adapted for the tubular fixed-bed due to nitrogen flow through the porous sample and *Laminar Flow* for the air domain around the quartz tube due to the natural convective cooling. The fluid dynamics are represented as time-dependent compressible fluid flow according to the following equations [31]:

$$\rho \frac{\partial}{\partial t} \mathbf{u} + \rho (\mathbf{u} \cdot \nabla) \mathbf{u} = \nabla \cdot \left[-p \mathbf{I} + \eta (\nabla \mathbf{u} + (\nabla \mathbf{u})^T) - \frac{2}{3} \eta (\nabla \cdot \mathbf{u}) \mathbf{I} \right] + \mathbf{F} \quad (5)$$

$$\frac{\partial}{\partial t} \rho + \nabla \cdot (\rho \mathbf{u}) = 0 \quad (6)$$

$$\frac{\rho}{\epsilon_{bed}} \left(\frac{\partial}{\partial t} \mathbf{u} + (\mathbf{u} \cdot \nabla) \frac{\mathbf{u}}{\epsilon_{bed}} \right) = \nabla \cdot \left[-p \mathbf{I} + \frac{\mu}{\epsilon_{bed}} (\nabla \mathbf{u} + (\nabla \mathbf{u})^T) - \frac{2\mu}{3\epsilon_{bed}} (\nabla \cdot \mathbf{u}) \mathbf{I} \right] - (\eta \kappa^{-1}) \mathbf{u} \quad (7)$$

Eq. (5) stands for the free flow in the quartz tube and the laminar flow for the air domain, see Fig. 2c and d. The first and second terms on the left-hand side are acceleration forces, and on the right side, there are pressure gradient and viscous forces. Conservation of mass is

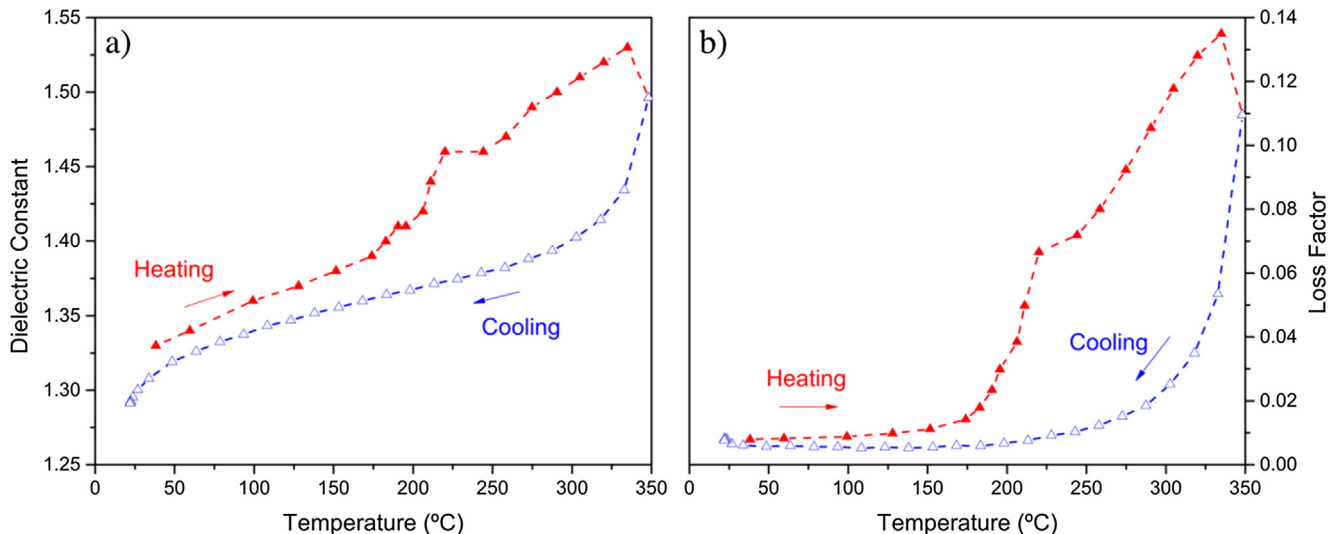


Fig. 3. Dielectric properties of NaY zeolite (a) Dielectric constant (b) Loss factor as a function of temperature.

expressed by the continuity equation, Eq. (6), which is derived by considering a unit volume of the medium and it states that the rate of increase of the mass of the fluid within an elementary unit equals to the net mass flux into the volume. Eq. (7) was used to describe the flow in the porous region, known as the *Brinkman equation* which is a combination of the continuity equation and the momentum equation. In this equation, ϵ_p and κ stand for the bed porosity and permeability, respectively, see Table 1 [31,32]. Following assumptions have been made:

- The nitrogen flow rate, 100 mL/min, pressure, 1 atm, and temperature, 20 °C, are fixed at the inlet of the quartz tube.
- No slip conditions, on the cylindrical wall of the quartz tube, $\mathbf{u} = 0$
- Since fluid dynamics and heat transfer are coupled, the sampling and IR camera ports, see Figs. 1a and 2b, were assigned as open boundaries because these ports are in contact with a large volume of fluid, i.e., surrounding air. In this way, fluid can both enter and leave the domain through these ports.
- The convective velocity field of air around the quartz tube wall is computed by applying a laminar flow model, considering the Rayleigh number criterion $Ra = Gr \cdot Pr < 1 \times 10^9$, where Gr and Pr are the Grashof and Prandtl numbers, respectively.
- A vertical buoyancy force term related to the thermal expansion is also included in Eq. (5) for the air domain around the quartz tube: $\mathbf{F} = -g(\rho_{air} - \rho_{air,ref})[\mathbf{N}/\text{m}^3]$, where g is the gravitational acceleration (9.81 m/s²) and ρ and ρ_{ref} are the simulated density and reference density of air, respectively (at atmospheric pressure and 20 °C).

4. Results and discussions

4.1. Dynamic measurement of dielectric properties

Before any measurement, the NaY zeolite was completely dried (see experimental section), Fig. 3 show the dielectric properties of NaY measured at 2.45 GHz as a function of temperature. When the zeolite is dehydrated (> 250 °C), the relaxation mechanism related to microwave heating is linked to the mobility of extra-framework cations to different ion exchange positions [38–40]. In this manner, Legras et al. [38] studied the dielectric properties for partially and fully hydrated FAU type zeolites in the 0.5 to 20 GHz microwave region at a fixed temperature of 20 °C. At low water loading, they observed a relaxation mechanism at peak frequencies between 1.4 and 1.6 GHz, which could be extended to 2.5 GHz with 15% changes in the loss factor. This mechanism is related to the phenomenon called space charge polarization that can be produced by the separation of mobile positively and negatively charged particles under an applied electric field. In the case of zeolites, the negative charge is in the oxygen atoms of the structure and the positive corresponds to extra-framework cations. Since the NaY zeolite used in this work (Si/Al = 2.5) contains 13.0 wt% of Na⁺ as an extra-framework cation, its contribution to the dielectric properties of low silica zeolite is the major phenomenon at 2.45 GHz. The data in the heating and cooling cycles were collected when the microwave is ON and OFF, respectively. The difference in the two cycles could be related to the influence of the MW field on the dielectric properties of the solid, since we are using a MW field to heat the sample. For this reason, to include only the effect of the temperature, on the dielectric properties, the values included in the simulation are the ones corresponding to the cooling cycle. According to the analyses, see Fig. 3, the loss factor in the heating cycle, when MW is ON, increased exponentially with temperature (> 200 °C), as a consequence of the fact that, as temperature increases, the motion of Na⁺ increases. This corresponds to thermal runaway and it was observed during experimentations in our lab with other microwave cavity, see Fig. S3-Supporting information. Once zeolite Y is dehydrated, the temperature continues rising up to around 200 °C and at this point the temperature sharply increases because the

power absorbed Q_{MW} increases, according to Eq. (3), and following the same trend as the loss factor values presented in Fig. 3b). The applied microwave power needs to be controlled properly in order to avoid the thermal runaway [38,41,42].

4.2. Three-dimensional finite element model, electromagnetic field distribution

When microwaves travel through the transmission lines, e.g., coaxial cable, waveguides, and enter to the microwave components, some energy enters and some is reflected due to the mismatch between the transmission lines and components. One way of analyzing microwave components is to relate the input and output variables of each component. Since the voltage and current cannot be measured at high frequencies, e.g., microwaves, S-parameters are often used to analyze microwave components. The S-parameters are defined in terms of wave variables, i.e., power, electric and magnetic fields, which can be easily measured at microwave frequencies by a vector network analyzer (VNA). Terminated transmission lines are considered one-port, and they are characterized by S-parameters in terms of S_{11} . The term S_{11} stands for the ratio of the reflected power to incident power. Since it is a ratio (non-dimensional parameter), it is usually given in logarithmic scale (in dB) to describe the magnitude of the S-parameters. This measurement is done with a certain frequency range, it is also known as reflection spectrum.

Reflection spectrums, S_{11} parameters, were experimentally measured and simulated with the regarding immersion depths of *stub 1* = 25.44 mm, *stub 2* = 27.57 mm and *stub 3* = 8.48 mm, see Fig. 1. The comparison between the measured and simulated data of S_{11} parameters are presented in Fig. 4. A shift in resonance frequency in the reflection spectrum is apparent between the empty and the cavity loaded with the quartz tube; resonance occurs at the frequency of minimum reflection. As the quartz tube was introduced inside the cavity it interacts with the electromagnetic field and changes its resonant behavior, the effect of which is apparent throughout the cavity and can therefore be registered at the cavity port as a change in the S_{11} parameter. The same phenomena were also observed in the simulation with a slight difference (magnitude and the frequency) in the case of loaded cavity. These matching spectral response and impedance matching characteristics show that the behavior of the microwave model agrees well with the physical setup which results in the validation of the model from the electromagnetic point of view.

The cross-section views of normalized electric field distributions along the y-direction inside the empty and loaded cavity are presented

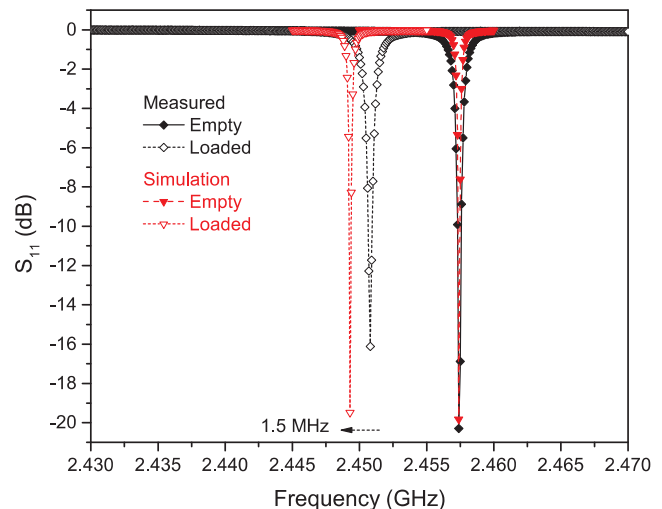


Fig. 4. Measured and Simulated S_{11} parameters (reflection spectrum) of empty and loaded cavity.

in Fig. 5. The introduction of the fixed-bed quartz tube affects the electric field distribution but the effect is not large due to the small size of the fixed-bed and the low values of the dielectric constant of the sample. This is also apparent in the relatively small shift in resonance frequency, see Fig. 4. The highest electric field intensity was observed at the frontier between the sample and the quartz wool (see Fig. 5d). This simulation also reveals that the fixed-bed quartz tube is effectively exposed to the maximum electric field intensity in the cavity.

4.3. Three-dimensional finite element model, temperature distribution

The experimental fixed-bed temperature data was registered by the fiber optic sensor at the bottom of the sample, where the temperature was highest, and the infrared camera was used to measure the outer surface temperature of the quartz wall. Transient temperature profiles show that the simulated data are in good agreement with the experimental ones, as shown in Fig. 6, where the predicted maximum temperatures for the fixed-bed and the quartz wall are represented, respectively. The average percentage relative deviations between the simulation and the experimental data of the fixed-bed and the surface temperatures were 10.3% and 13.4%, respectively. This over prediction of the temperature could be related to the lower reflection power observed in the simulations of the loaded cavity compared to the experimental value (see Section 4.2). However, to account or this we already adjust the input power with a ratio between the measured and simulated S_{11} parameters of the loaded cavity, see Fig. 4. The input power used in simulations was 26 W instead of 30 W. Also, the

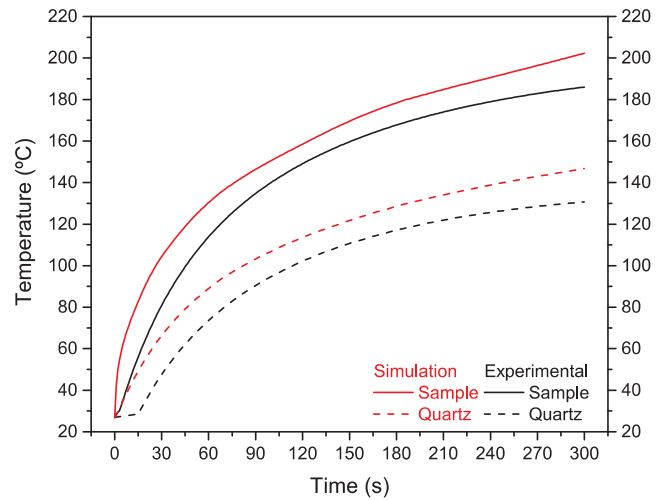


Fig. 6. Comparison of the experimental measurements and simulation predictions of transient maximum temperature profiles of the fixed-bed (measured with the fiber optic sensor) and the quartz wall (measured with the infrared thermographic camera).

discrepancy between measured and experimental valued could be attributed to the material properties such as thermal conductivity of the zeolite and quartz tube. In the case of zeolites, various thermal conductivities have been reported by many researchers, some of them

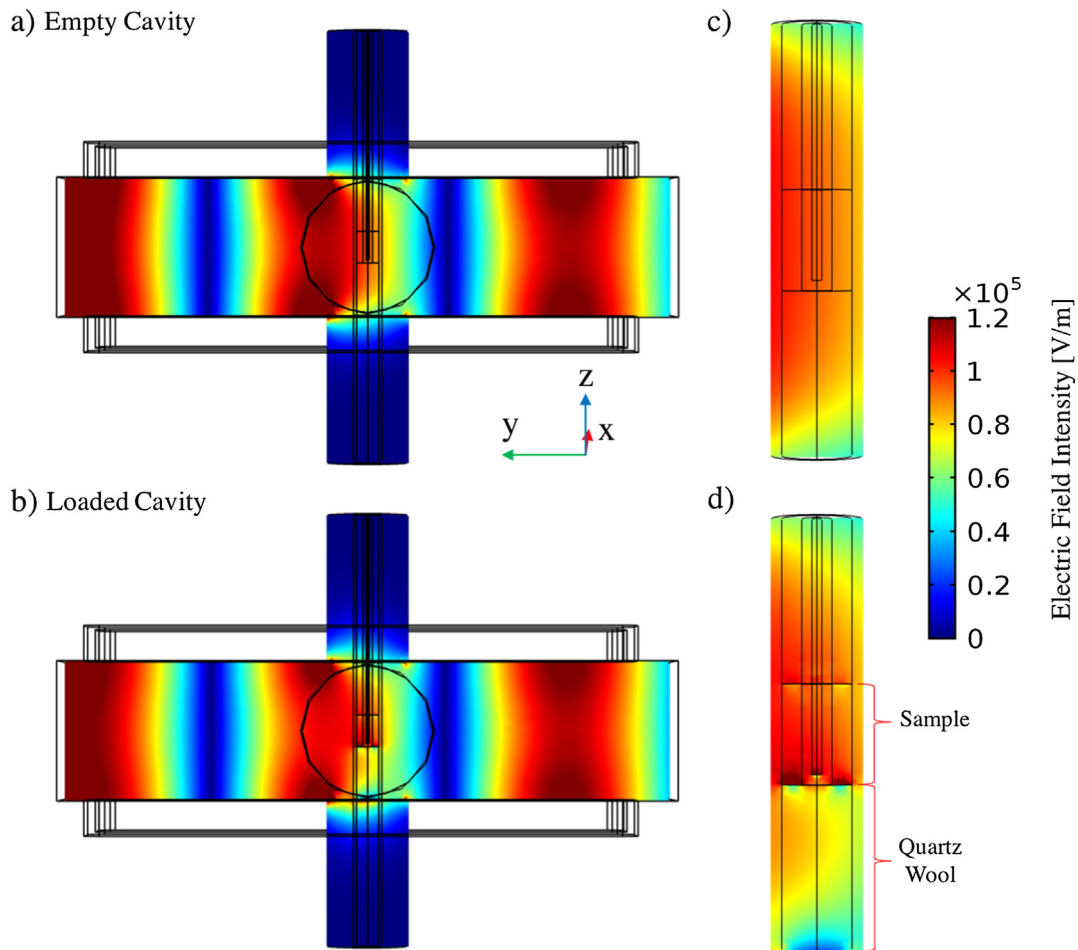


Fig. 5. Simulated electric field distribution inside the (a) empty and (b) loaded cavity and close look to corresponding quartz tube locations inside the cavity when it is (c) empty and (d) loaded. For clarity, in (b) and (d) quartz tube and fixed-bed domains are maintained in the case of empty cavity with the properties of air ($\epsilon' = 1$, $\epsilon'' = 0$, $\mu_r = 1$, and $\sigma = 0$) to have the same number of elements.

ranges in between 0.15 and 0.30 W/(m K) [35,43–45] which results in simulated final temperatures of 203 and 173 °C, respectively, see Fig. S1-Supporting information. Despite the inaccuracy possibly involved with the emissivity and the sensor calibration, these matching temperature data results the validation of the developed three-dimensional finite element model from the heat transfer point of view.

Fig. 7 shows the surface temperature of the quartz wall measured by an infrared camera at different time periods and the corresponding simulated data. The predictions are in good agreement with experimental data; in both cases, the sample starts heating from the center and then it expands axially. Even though the infrared camera has a limited resolution (320×240 pixel), it can be observed that the left side of the quartz tube has a slightly higher temperature (Fig. 7b, at 30 s, ca. 2 °C).

The simulated radial temperature distribution inside the quartz tube as well as along the sample at steady-state is depicted in Fig. 8c. The radial temperature profiles show that the temperature is considerably lower at the outer layers, compared to the center of the quartz tube. This is because of heat is absorbed in the volume of the sample under microwave irradiation and then lost by natural convection along the surface of the quartz tube to the surrounding air. The variation of radial temperature profiles at different heights in the fixed-bed quartz tube is shown in Fig. 8d. There is a slight temperature increase, ca. 2–4 °C, at the left side (1–3 mm, towards the generator side) of the sample in comparison to the right side (6–8 mm). This is in accordance with the electrical field distribution in the cavity, which is not centered within the fixed-bed, explained previously, see Fig. 8a. Despite a distribution that tends towards the generator side, i.e., left side, the overall temperature distribution is roughly symmetrical, i.e., the asymmetry of the electrical field is smoothed out by heat transfer. The temperature difference is less pronounced at the top ($H = 10$ mm) compared to the bottom of the sample ($H = 0$ mm), and the bottom part is hotter than the top, ca. 40 °C. The maximum radial temperature is reached near the fiber optic sensor location, 4–5 mm. This temperature gradient is linked to the non-uniform electric field distribution inside the sample in conjunction with the loss factor of the zeolite fixed-bed. This can be seen as a volumetric power dissipation in Fig. 8b. It should be noted that the high-temperature region corresponds to the relatively high electric field region, see Fig. 8a and b [24,46]. Despite this electric field gradient, it was observed that 58% of the fixed bed has the temperature range in between 160 and 197 °C.

4.4. Three-dimensional finite element model, fluid dynamics

The single-phase laminar flow equations of cooling air outside the quartz tube walls were computed to account for the natural cooling. The velocity field of the surrounding air and the temperature field are depicted in Fig. 9. The velocity field distribution is represented as an arrow volume and 2-D cross-section, and the color expression reflects the magnitude of the velocity field in m/s, see Fig. 9a and b. The results show that the surrounding air enters through the IR camera and bottom sampling ports and circulates around the quartz tube walls. Then, the heated air goes out through the top sampling port. The same phenomenon can be also seen in the 2D flow field, see Fig. 9b. The temperature of the surrounding air reaches up to 150 °C in the vicinity of the quartz tube where the sample is located (Fig. 9c).

Local effects of the surrounding air of the quartz tube walls were accounted with modelling the convective velocity and temperature fields instead of using a stationary cooling model (i.e., constant heat transfer coefficient). The calculated average heat transfer coefficient distribution along the height of the quartz tube wall was 10.93 W/(m K).

Concerning the effect of the total flow of gases through the fixed bed in temperature distribution, we conducted a parametric study varying N_2 inlet flow rate from 50 to 200 mL/min (see Fig. S2) and no significant differences were observed, only with the 200 mL/min flow rate the temperature is slightly lower. These results could be expected since most of the MW energy is absorbed and dissipated in the form of heat within the zeolite solid, then this heat is transfer to the surrounding flow, since the heat capacity of gases is very low the effect of increasing the flow only affects slightly the final temperature achieved.

4.5. Parametric studies

The overall energy balance in the microwave heating cavity and the fixed-bed shows that only 6.2% of the input power was dissipated within the NaY zeolite fixed-bed, with a reflection loss of 1.2%. This means that the rest of the microwave energy was dissipated in the metallic cavity wall due to electric currents. The interpretation of the efficiency of this microwave heating cavity is related to the physical dimensions of the cavity and the small volume of the NaY zeolite fixed-bed (0.31 mL with respect to the whole cavity volume, 2.8L) in the

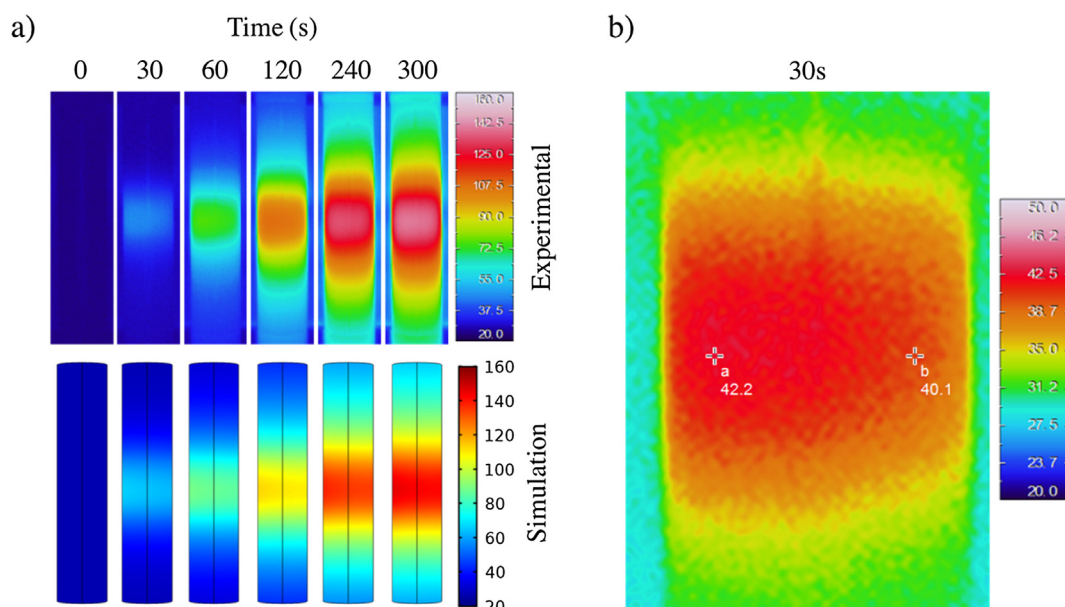


Fig. 7. Infrared images of the quartz surface temperature at different time periods and corresponding simulated data, (b) an infrared image at 30 s, color legends are in °C.

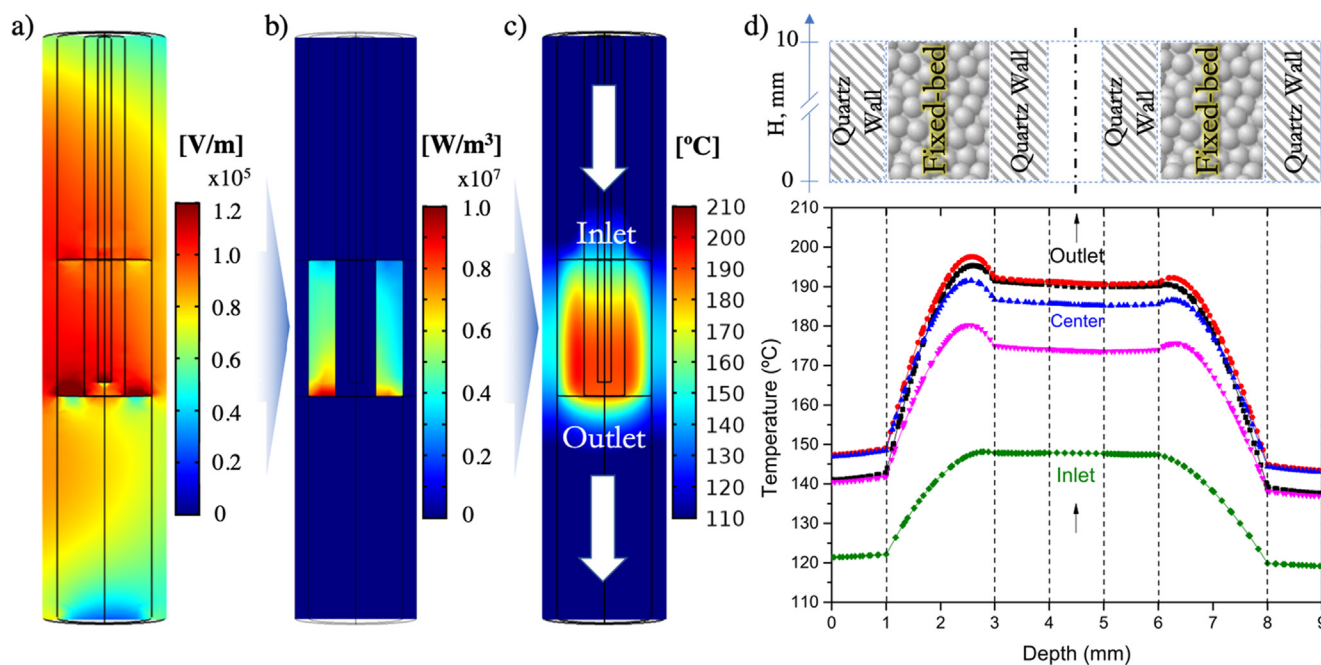


Fig. 8. Simulated cross-sectional view of the quartz tube fixed-bed and its corresponding (a) electric field (b) power (c and d) spatial temperature distribution at steady-state.

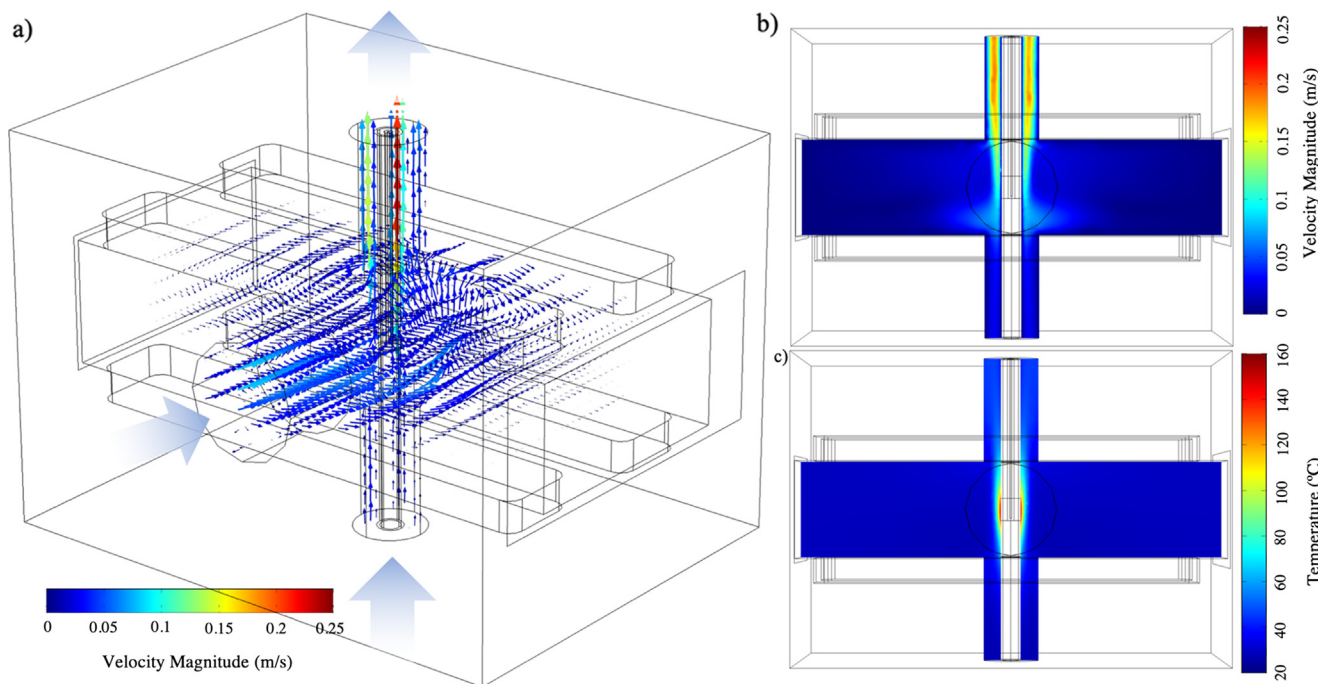


Fig. 9. Simulated convective velocity field of surrounding air inside the cavity (a) arrow volume and (b) 2-D cross-sectional representation and (c) temperature field at $t = 300$ s, average quartz tube wall temperature:200 °C.

microwave heating cavity. A similar conclusion was reached by Coss et al. [47], only 27% of the input power was absorbed in their case, even though they used a larger bed of a good microwave absorber, granulated activated carbon and the adsorbent volume = 18.8 mL. The authors expected that this efficiency could become higher with the larger volume of adsorbent. Also, Cherbanski [48] calculated the efficiency factor using 13X zeolite in a multi-mode cavity, giving a 21% efficiency (adsorbent volume = 253 mL). We decided to simulate larger volumes of the same adsorbent, in our microwave heating cavity, to predict its efficiency. The inner diameter of the quartz tube was

increased from 7 mm (V:0.31 mL) to 10 (V:0.71 mL) and 14 mm (V:1.47 mL). Fig. 10 represents the parametric analysis, power dissipation and corresponding electric field distributions of different volumes of adsorbent. The results show that 13.8 and 25.1% of the input power could be dissipated if the adsorbent volume was increased to 0.71 and 1.47 mL, respectively. Even though the resonance frequencies of larger volumes of adsorbent were shifted to the lower frequencies, see Fig. 10a, they were still in the solid-state microwave generator's spectral band, which is from 2.43 to 2.47 GHz. Thus, the matching basically can be done by simply modifying the supplied frequency to

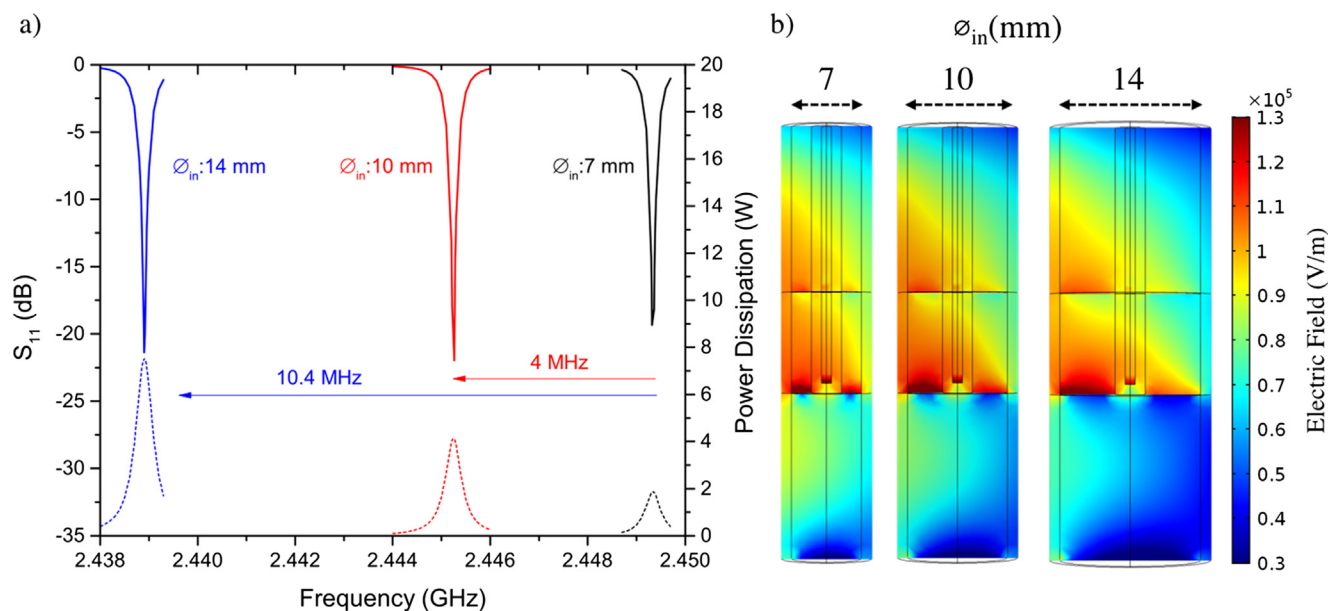


Fig. 10. Simulated (a) reflection spectrum (S_{11} parameters) and power dissipation as a function of the excitation frequency with (b) corresponding electric field distribution of larger volumes of absorbent with an input power of 30 W.

the cavity. It was observed that less than 1 MHz deviation from the nominal frequency is sufficient to change the dissipated power by 14–27%. Cherbanski et al. [36] also observed the same behavior for the microwave heating of water in a single-mode applicator; they concluded that a minor 5 MHz deviation from the nominal frequency caused about 20% variation of the absorbed microwave power.

As it was mentioned in the introduction the evolution of the dielectric properties with temperature would result in a temperature runaway in the sample that it could be predicted with the simulation. In Fig. 11a, it could be observed that when the input power of the microwave cavity increases up to 38 W the temperature rises sharply after 210 s heated. A closed up of the power dissipation and temperature distribution in these two cases is presented in Fig. 11b.

Different materials such as silicon carbide, SiC, ($\epsilon' = 16.9$ and $\epsilon'' = 0.77$, V:0.31 mL) and carbon nanotubes, CNTs, ($\epsilon' = 17.8$ and $\epsilon'' = 26.4$, V = 0.31 mL) were also employed in the simulation due to their relatively higher dielectric properties as compared to NaY zeolite ($\epsilon' = 1.3$ and $\epsilon'' = 0.01$, V:0.31 mL). Dielectric properties of CNTs and SiC as a function of temperature were presented in Fig. S4-supporting information. Fig. 12 represents the parametric sweep of two

different samples. It was observed that 16.3 and 49.2% of the input power were dissipated in the CNTs and SiC fixed-beds, respectively. The electric field intensity decreased by two orders of magnitude, especially in the case of CNTs, see Fig. 12b. This is due to the high dielectric properties, which reduce the penetration depth of the electromagnetic waves into the load.

5. Conclusions

In this study, microwave heating of dry porous NaY zeolite was investigated numerically and experimentally. A three-dimensional mathematical model of the microwave heating system with the fixed-bed tubular configuration was developed. Energy and momentum equations were solved together with Maxwell's equations using COMSOL MULTIPHYSICS® software. The electric field distribution in the microwave heating cavity, as well as in the fixed-bed, and the reflection spectrum were obtained. Furthermore, the transient temperature profiles of the zeolite and quartz tube were simulated on the basis of experimentally measured dielectric properties (ϵ' and ϵ'') as a function of temperature.

The numerical results of the reflection spectra and transient

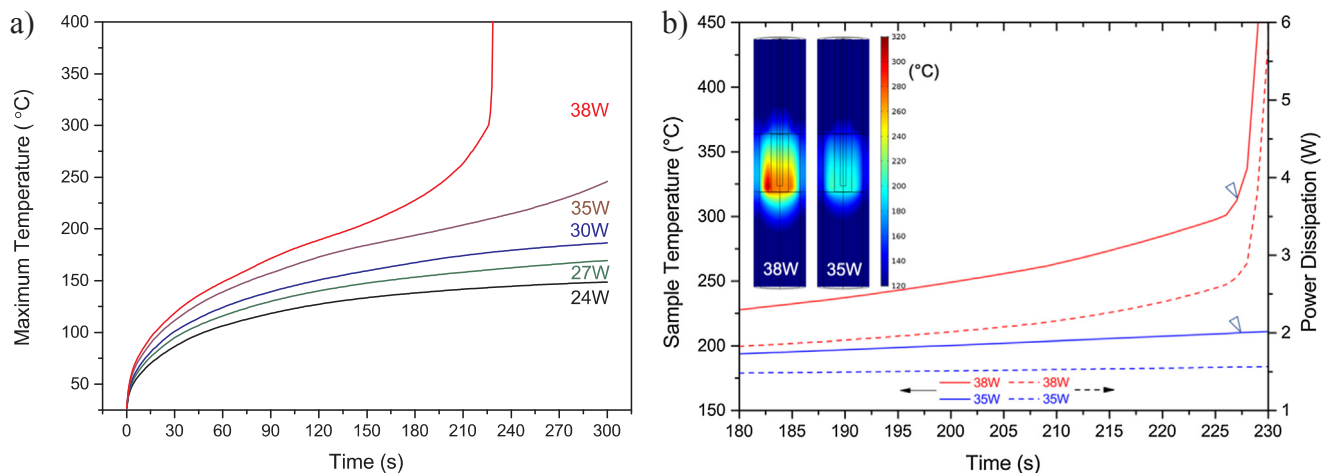


Fig. 11. Simulation of temperature evolution with time for different MW power. (b) Transient temperature profiles and power dissipation at different incident MW power. (inset: at the time 227 s. when the thermal runaway starts).

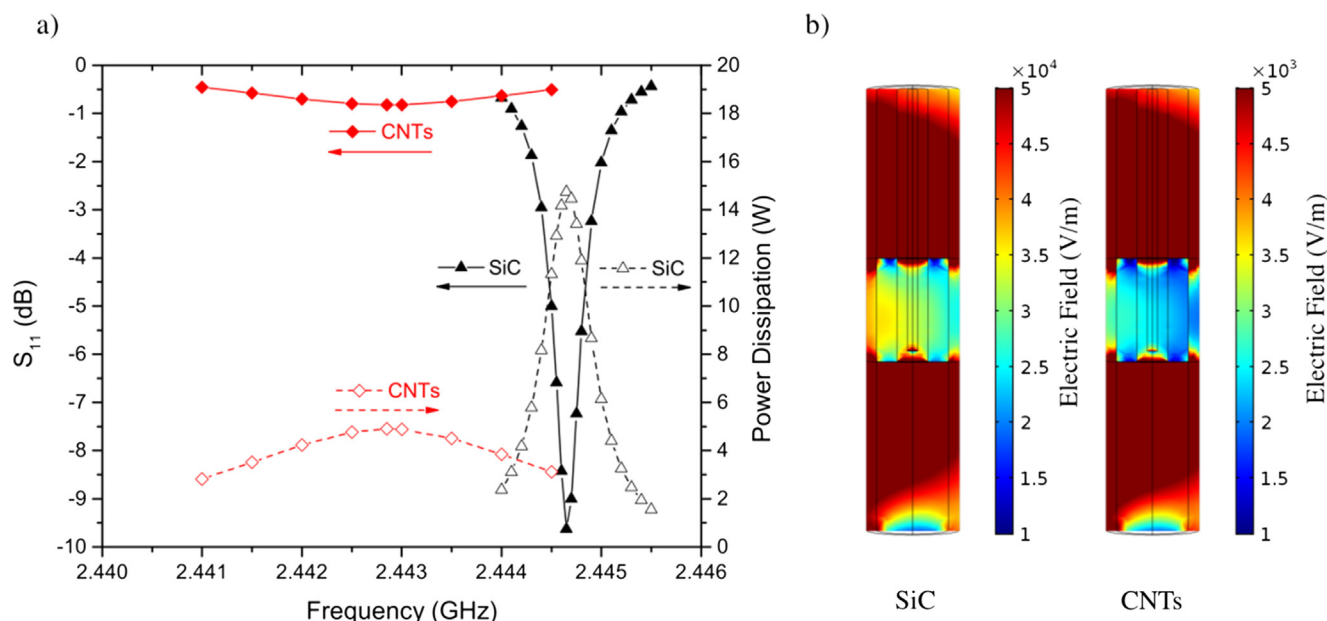


Fig. 12. Simulated (a) reflection spectrum (S_{11} parameters) and power dissipation and (b) corresponding electric field distribution of SiC and CNTs with an input power of 30 W (ϕ in: 7 mm).

temperature profiles of the fixed-bed and quartz wall surface perfectly matched with the experimental data. An average percentage relative deviation of 10.3% for the fixed-bed and 13.4% for the quartz wall was observed. Due to the non-uniform electric field distribution within the sample, a temperature gradient was observed. Despite this gradient, 58% of the fixed bed has a temperature between 160 and 197 °C.

The simulation results show that the energy efficiency of the existing microwave heating cavity could be increased by using larger volumes of the NaY zeolite load, as well as heating materials with higher dielectric loss compared to zeolite such as SiC and CNTs. Furthermore, this finite element analysis technique can be used for evaluation of alternative materials and/or reactor designs.

Acknowledgements

Financial support from the European Research Council ERC-Advanced Grant HECTOR-267626 is gratefully acknowledged. Hakan Nigar acknowledges financial support from the Spanish Ministry of Education for the FPU grant (Formación del Profesorado Universitario – FPU12/06864), and also for the academic short stay grant (Estancia Breve – FPU2016) at the Delft University of Technology, Delft, The Netherlands.

Appendix A. Supplementary material

Supplementary data to this article can be found online at <https://doi.org/10.1016/j.applthermaleng.2019.03.117>.

References

- [1] J.M. Bermúdez, D. Beneroso, N. Rey-Raap, A. Arenillas, J.A. Menéndez, Energy consumption estimation in the scaling-up of microwave heating processes, *Chem. Eng. Process.: Process Intensif.* 95 (2015) 1–8.
- [2] J.D. Moseley, C.O. Kappe, A critical assessment of the greenness and energy efficiency of microwave-assisted organic synthesis, *Green Chem.* 13 (2011) 794–806.
- [3] R.J. Meredith, *Institution of Electrical Engineers' Handbook of Industrial Microwave Heating*, Institution of Electrical Engineers, (1998).
- [4] L. Xu, C. Srinivasakannan, J. Peng, S. Guo, H. Xia, Study on characteristics of microwave melting of copper powder, *J. Alloys Compd.* 701 (2017) 236–243.
- [5] G.D. Stefanidis, A.N. Munoz, G.S.J. Sturm, A. Stankiewicz, A helicopter view of microwave application to chemical processes: reactions, separations, and equipment concepts, *Rev. Chem. Eng.* 30 (2014) 233–259.
- [6] T. Durka, G.D. Stefanidis, T. Van Gerven, A.I. Stankiewicz, Microwave-activated methanol steam reforming for hydrogen production, *Int. J. Hydrogen Energy* 36 (2011) 12843–12852.
- [7] G.S.J. Sturm, M.D. Verweij, T. van Gerven, A.I. Stankiewicz, G.D. Stefanidis, On the effect of resonant microwave fields on temperature distribution in time and space, *Int. J. Heat Mass Transf.* 55 (2012) 3800–3811.
- [8] G.S.J. Sturm, M.D. Verweij, Gerven Tv, A.I. Stankiewicz, G.D. Stefanidis, On the parametric sensitivity of heat generation by resonant microwave fields in process fluids, *Int. J. Heat Mass Transf.* 57 (2013) 375–388.
- [9] A. Ramírez, J.L. Hueso, R. Mallada, J. Santamaría, Ethylene epoxidation in microwave heated structured reactors, *Catal. Today* 273 (2016) 99–105.
- [10] S. Horikoshi, M. Kamata, T. Sumi, N. Serpone, Selective heating of Pd/AC catalyst in heterogeneous systems for the microwave-assisted continuous hydrogen evolution from organic hydrides: Temperature distribution in the fixed-bed reactor, *Int. J. Hydrogen Energy* 41 (2016) 12029–12037.
- [11] R.M.C. Mimoso, D.M.S. Albuquerque, J.M.C. Pereira, J.C.F. Pereira, Simulation and control of continuous glass melting by microwave heating in a single-mode cavity with energy efficiency optimization, *Int. J. Therm. Sci.* 111 (2017) 175–187.
- [12] B. Lin, H. Li, Z. Chen, C. Zheng, Y. Hong, Z. Wang, Sensitivity analysis on the microwave heating of coal: a coupled electromagnetic and heat transfer model, *Appl. Therm. Eng.* 126 (2017) 949–962.
- [13] B.Q. Lin, H. Li, H.M. Dai, C.J. Zhu, H. Yao, Three-dimensional simulation of microwave heating coal sample with varying parameters, *Appl. Therm. Eng.* 93 (2016) 1145–1154.
- [14] S. Farag, A. Sobhy, C. Akyel, J. Doucet, J. Chaouki, Temperature profile prediction within selected materials heated by microwaves at 2.45GHz, *Appl. Therm. Eng.* 36 (2012) 360–369.
- [15] L. Acevedo, S. Usón, J. Uche, Numerical study of cullet glass subjected to microwave heating and SiC susceptor effects. Part I: combined electric and thermal model, *Energy Convers. Manage.* 97 (2015) 439–457.
- [16] H. Demir, The effect of microwave regenerated adsorbent bed on the performance of an adsorption heat pump, *Appl. Therm. Eng.* 50 (2013) 134–142.
- [17] H. Demir, Development of microwave assisted zeolite–water adsorption heat pump, *Int. J. Refrig.* 36 (2013) 2289–2296.
- [18] G. Gediz Ilis, H. Demir, Influence of bed thickness and particle size on performance of microwave regenerated adsorption heat pump, *Int. J. Heat Mass Transf.* 123 (2018) 16–24.
- [19] H. Awala, J.P. Gilson, R. Retoux, P. Boullay, J.M. Goupil, V. Valtchev, et al., Template-free nanosized faujasite-type zeolites, *Nat. Mater.* 14 (2015) 447–451.
- [20] Database of Zeolite Structures, <http://www.iza-structure.org/databases>.
- [21] H. Nigar, N. Navascués, O. de la Iglesia, R. Mallada, J. Santamaría, Removal of VOCs at trace concentration levels from humid air by microwave swing adsorption, kinetics and proper sorbent selection, *Sep. Purif. Technol.* 151 (2015) 193–200.
- [22] H. Nigar, I. Julián, R. Mallada, J. Santamaría, Microwave-assisted catalytic combustion for the efficient continuous cleaning of VOC-containing air streams, *Environ. Sci. Technol.* 52 (2018) 5892–5901.
- [23] J.M. Catala-Civera, A.J. Canos, P. Plaza-Gonzalez, J.D. Gutierrez, B. Garcia-Banos, F.L. Penaranda-Foix, Dynamic measurement of dielectric properties of materials at high temperature during microwave heating in a dual mode cylindrical cavity microwave theory and techniques, *IEEE Trans.* 63 (2015) 2905–2914.
- [24] W.-H. Chen, T.-C. Cheng, C.-I. Hung, Numerical predictions on thermal characteristic and performance of methanol steam reforming with microwave-assisted heating, *Int. J. Hydrogen Energy* 36 (2011) 8279–8291.

- [25] G.S.J. Sturm, M.D. Verweij, A.I. Stankiewicz, G.D. Stefanidis, Microwaves and microreactors: design challenges and remedies, *Chem. Eng. J.* 243 (2014) 147–158.
- [26] D.M. Pozar, *Microwave Engineering*, 4th ed., Wiley, Hoboken, 2012.
- [27] G.S.J. Sturm, A.Q. Van Braam Houckgeest, M.D. Verweij, T. Van Gerven, A.I. Stankiewicz, G.D. Stefanidis, Exploration of rectangular waveguides as a basis for microwave enhanced continuous flow chemistries, *Chem. Eng. Sci.* 89 (2013) 196–205.
- [28] RF Module User's Guide, pp. 80–82. COMSOL Multiphysics® v. 5.2. www.comsol.com. COMSOL AB, Stockholm, Sweden.
- [29] Heat Transfer Module User's Guide, pp. 105–110. COMSOL Multiphysics® v. 5.2. www.comsol.com. COMSOL AB, Stockholm, Sweden.
- [30] B. Legras, I. Polaert, M. Thomas, L. Estel, About using microwave irradiation in competitive adsorption processes, *Appl. Therm. Eng.* 57 (2013) 164–171.
- [31] CFD Module User's Guide, pp. COMSOL Multiphysics® v. 5.2. www.comsol.com. COMSOL AB, Stockholm, Sweden.
- [32] D.A. Nield, A. Bejan, *Convection in Porous Media*, Springer, New York, 2012.
- [33] A.S. Pushnov, Calculation of average bed porosity, *Chem. Petrol. Eng.* 42 (2006) 14–17.
- [34] C. Pan, M. Hilpert, C.T. Miller, Pore-scale modeling of saturated permeabilities in random sphere packings, *Phys. Rev. E – Statist., Nonlinear, Soft Matt. Phys.* 64 (2001) 066702/1–/9.
- [35] K.C. Leong, Y. Liu, Numerical modeling of combined heat and mass transfer in the adsorbent bed of a zeolite/water cooling system, *Appl. Therm. Eng.* 24 (2004) 2359–2374.
- [36] R. Cherbański, L. Rudniak, Modelling of microwave heating of water in a mono-mode applicator – influence of operating conditions, *Int. J. Therm. Sci.* 74 (2013) 214–229.
- [37] I.P. Iliev, S.G. Gocheva-Ilieva, Self-consistent analytical model of the radial temperature profile of a high-powered He–SrBr 2 laser, *Opti. Quant. Electron.* 48 (2016).
- [38] B. Legras, I. Polaert, L. Estel, M. Thomas, Mechanisms responsible for dielectric properties of various faujasites and linde type a zeolites in the microwave frequency range, *J. Phys. Chem. C* 115 (2011) 3090–3098.
- [39] J. Gracia, M. Escuin, R. Mallada, N. Navascues, J. Santamaría, Heating of zeolites under microwave irradiation: a density functional theory approach to the ion movements responsible of the dielectric loss in Na, K, and Ca A-zeolites, *J. Phys. Chem. C* 117 (2013) 15659–15666.
- [40] U. Simon, U. Flesch, Cation-cation interaction in dehydrated zeolites X and Y monitored by modulus spectroscopy, *J. Porous Mater.* 6 (1999) 33–40.
- [41] T. Ohgushi, M. Nagae, Durability of zeolite against repeated activation treatments with microwave heating, *J. Porous Mater.* 12 (2005) 265–271.
- [42] O. Tatsuo, W. Akiko, Simple suppressing method of thermal runaway in microwave heating of zeolite and its application, *PhysChemComm* 4 (2001) 18–20.
- [43] A. Griesinger, K. Spindler, E. Hahne, Measurements and theoretical modelling of the effective thermal conductivity of zeolites, *Int. J. Heat Mass Transf.* 42 (1999) 4363–4374.
- [44] M.B. Jakubinek, B.-Z. Zhan, M.A. White, Temperature-dependent thermal conductivity of powdered zeolite NaX, *Micropor. Mesopor. Mater.* 103 (2007) 108–112.
- [45] Z.Y. Liu, G. Cacciola, G. Restuccia, N. Giordano, Fast simple and accurate measurement of zeolite thermal conductivity, *Zeolites* 10 (1990) 565–570.
- [46] W.-H. Chen, H.-J. Liou, C.-I. Hung, A numerical approach of interaction of methane thermocatalytic decomposition and microwave irradiation, *Int. J. Hydrogen Energy* 38 (2013) 13260–13271.
- [47] P.M. Coss, C.Y. Cha, Microwave regeneration of activated carbon used for removal of solvents from vented air, *J. Air Waste Manage Assoc.* 50 (2000) 529–535.
- [48] R. Cherbański, Calculation of critical efficiency factors of microwave energy conversion into heat, *Chem. Eng. Technol.* 34 (2011) 2083–2090.